Sensorless Integral Sliding Mode Control of Single-Phase Grid-Connected PV System

El Otmani, F.; Abouloifa, A.; Aourir, M.; Lachkar, I.; Katir, H.; Noussi, K.; Assad, F.; Giri, F.; Guerrero, J. M.

Published in:
IFAC-PapersOnLine

DOI (link to publication from Publisher):
10.1016/j.ifacol.2021.12.009

Publication date:
2021

Document Version
Publisher's PDF, also known as Version of record

Available online at www.sciencedirect.com

ScienceDirect

IFAC Papers Online CONFERENCE PAPER ARCHIVE

IFAC PapersOnLine 54-21 (2021) 49–54

Sensorless Integral Sliding Mode Control of Single-Phase Grid-Connected PV System

F. El Otmani * **A. Abouloifa** * **M. Aourir** * **I. Lachkar** **
H. Katir * **K. Noussi** * **F. Assad** * **F. Giri** *** **JM. Guerrero** ****

* *TI Lab, Department of Physics, FSBM, Hassan II University of Casablanca, Morocco (fadwa.elotmani@gmail.com).*
** *LESE Lab, ENSEM Casablanca, Morocco*
*** *Normandie UNIV, UNICAEN, ENSICAEN, 14000 Caen, France*
**** *Department of Energy Technology, 9220 Aalborg East, Denmark*

Abstract: This paper presents a grid-connected photovoltaic (PV) system. The conversion scheme consists of a three-level boost converter (TLBC), a half-bridge inverter (HBI), and an LCL filter to adapt the PV energy and inject it into the grid with low total harmonic distortion (THD) and unity power factor (PF). This study aims to achieve four main objectives: i) Ensure maximum available PV power with high robustness against environmental variations, ii) Guarantee PF correction (PFC) where the output current must have a sinusoidal waveform in phase with the grid voltage, iii) Regulate the DC link voltage to follow a defined reference, iv) Ensure balance between TLBC output voltages. To achieve the mentioned objectives, a nonlinear controller based on the integral sliding mode approach (ISM) is developed. In addition, a Kalman observer is designed to estimate the PV voltage and current in order to reduce the number of physical sensors and thus the cost and space of the studied system. Then, based on the PV current and voltage estimated by the designed observer, a sensorless maximum power point tracker (MPPT) based on the INC & COND algorithm is implemented to extract the maximum PV power despite changing weather conditions. Simulation results were performed in the Matlab/Simulink/SimPowerSystems environment to evaluate the proposed control strategy and observer. These results demonstrate that the proposed controller and observer achieve the set objectives under standard and changing climate conditions.

Keywords: Photovoltaic system, Three-level boost, Electrical grid, Integral Sliding mode, Control of renewable energy resources, Application of power electronics, Kalman observer.

1. INTRODUCTION

The renewable energy (RE) solution offers a considerable variety of energy sources to replace fossil sources, feed the global market and meet energy needs. Among the RE sources, solar energy (SE) has attracted a lot of interest thanks to its clean, quiet and abandant energy. The main application of SE has been demonstrated in grid-connected PV systems, where power electronics play a critical role in extracting maximum power from the PV Aourir et al. (2020). In fact, PV power depends on climatic conditions such as temperature and irradiation. Therefore, a tracking algorithm is needed to guarantee the maximum PV power despite changing weather conditions. Several MPPT methods have been proposed in the literature, such as perturb and observe algorithm Alik and Jusoh (2018), incremental conductance algorithm Shahid et al. (2018), and Fuzzy Logic MPPT method Yilmaz et al. (2018). However, all of these algorithms require the measurement of PV current and voltage using sensors that scale to the resolution of the controller analog-to-digital converter (ADC). These sensors make the system bulky, expensive and take up a large place. Moreover, Hall-effect sensors are typically used to measure PV current. These sensors are sensitive and can be easily affected by external or stray magnetic fields, which could deflect the PV generator from the MPP and reduce the PV generation efficiency Das et al. (2018). Therefore, to ensure efficient use of the PV power, it is necessary to estimate the PV current and voltage to track the MPP. This issue has been extensively studied in the literature using different estimation techniques, as in Das et al. (2018), where the authors proposed an MPPT based P&O algorithm to estimate the PV current using the Luenberger observer technique. In Stitou et al. (2019), the authors discuss an output feedback control of sensorless PV systems based on the high gain observer technique for estimating PV current and voltage.

This study suggests a complete grid-connected PV generator. PV systems are typically connected to the grid via two stages: a DC-DC converter and a DC-AC converter to extract, adapt and stabilize PV energy, and then inject it into the electrical grid with low THD and unity PF. Previous studies have proposed various structures and controllers to deal with the complications of grid-connected PV system. Yahya et al. (2018) proposed a grid-connected PV system driven by microinverters where the system is controlled employing the backstepping approach, and the authors addressed the MPPT problem by investing a voltage reference optimizer. Abouloifa et al. (2018) discussed

10.1016/j.ifacol.2021.12.009

a PV system controlled using the SM approach and an adaptive observer to estimate unknown and inaccessible parameters. Barman et al. (2018) presented the design of a damping and passivity assignment-based control strategy (IDA-PBC) to control a PV system interfaced by a grid-connected inverter. Finally, Aourir et al. (2020) presented a topology consisting of two PV panels, a single-phase HBI using two DC link capacitors, and a grid-connected LCL filter, where the authors proposed a multi-loop controller designed based on the backstepping and Lyapunov approaches.

In this study, the conversion chain of the studied system consists of TLBC, HBI and an LCL filter. The main contributions of this paper are listed as follows:

- Sensorless MPP tracking based on PV current and voltage estimation.
- The use of a TLB converter offers a reduced inductance and a switching voltage rating equal to the half output voltage of the conventional boost converter.

This paper focuses on the control of the grid-connected PV system. Therefore, a multi-loop ISM controller (ISMC) has been designed to manage the energy between the PV generator and the electrical grid. The behavior of the proposed system is evaluated by different study cases. The robustness and reliability of the proposed control strategy and observer have been realized in Matlab/SimPowerSystems environment and proven under standard conditions and then under climatic variations.

The rest of the paper is organized as follows: The PV system is described and modeled in Section II. Section III is devoted to the design of the observers. Section IV is devoted to the development of a nonlinear controller based on the sliding mode approach. Then, the effectiveness of the proposed controller is examined by simulation results in Section V. Finally, a conclusion is drawn to summarize the overall study, and a list of references ends the paper.

2. SYSTEM DESCRIPTION AND MODELING

2.1 System Description

The suggested structure consists of a PV generator attached to a TLBC via the capacitor C_{pv}, then connected to a HBI through a DC link, and an LCL filter to reduce the current ripple cutting. The control inputs as they appear on the system topology illustrated in Fig. 1 are $[\mu, \mu_1, \mu_2]$. where, i_{pv} and v_{pv} are respectively the current and the

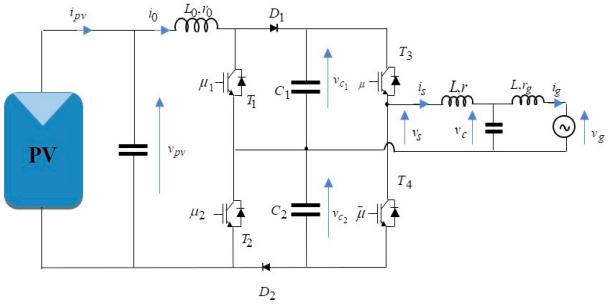

Fig. 1. Scheme of PV connected to a single-phase grid

voltage generated by the PV array; i_0 is the TLBC input current; v_{c_1} and v_{c_2} denote the series voltage of the DC link; i_s and v_c are respectively the current in L (the input of the LCL filter), and the voltage across C; i_g and v_g present respectively the current and the voltage of the grid; μ, μ_1, and μ_2 denote the continuous input signals of the system.

2.2 System Modeling

Instantaneous model: Applying standard Kirchhoff's Laws to the grid-connected PV system, the mathematical model turns out to be the following nonlinear differential equations system:

Subsystem 1:

$$L\frac{di_g}{dt} = -r_g i_g + v_c - v_g \tag{1a}$$

$$C\frac{dv_c}{dt} = i_s - i_g \tag{1b}$$

$$L\frac{di_s}{dt} = \frac{1+\mu}{2}v_{c_1} - \frac{1-\mu}{2}v_{c_2} - v_c - ri_s \tag{1c}$$

Subsystem 2:

$$C_{pv}\frac{dv_{pv}}{dt} = i_{pv} - i_0 \tag{2a}$$

$$L_0\frac{di_0}{dt} = v_{pv} - (1-\mu_1)v_{c_1} - (1-\mu_2)v_{c_2} - r_0 i_0 \tag{2b}$$

$$\frac{di_{pv}}{dt} = \vartheta(t) \tag{2c}$$

Subsystem 3:

$$C_1\frac{dv_{c_1}}{dt} = (1-\mu_1)i_0 - \frac{1+\mu}{2}i_s \tag{3a}$$

$$C_2\frac{dv_{c_2}}{dt} = (1-\mu_2)i_0 + \frac{1-\mu}{2}i_s \tag{3b}$$

$\vartheta(t)$ is a bounded real unknown signal that depends on the characteristics of the PV generator and the weather variations.

Average model: To avoid problems caused by binary control signals in the model (1-3), the system can be described by the average model, which is easily obtained by replacing each state variable by its average value and assuming that $C_1 = C_2 = C_{eq}$. Then, the average model is expressed as follows:

Subsystem 1:

$$L\dot{x}_1 = -r_g x_1 + x_2 - \bar{v}_g \tag{4a}$$

$$C\dot{x}_2 = x_3 - x_1 \tag{4b}$$

$$L\dot{x}_3 = 0.5\,(uw_1 + w_2) - x_2 - rx_3 \tag{4c}$$

Subsystem 2:

$$C_{pv}\dot{z}_1 = z_3 - z_2 \tag{5a}$$

$$L_0\dot{z}_2 = z_1 - r_0 z_2 - w_1 + 0.5\,(u_s w_1 - u_d w_2) \tag{5b}$$

$$\dot{z}_3 = \upsilon \tag{5c}$$

Subsystem 3:

$$C_{eq}\dot{w}_1 = (2-u_s)z_2 - ux_3 \tag{6a}$$

$$C_{eq}\dot{w}_2 = u_d z_2 - x_3 \tag{6b}$$

where, x_1, $\bar{v}_g$, x_2, x_3, z_1, z_2, z_3, w_1, w_2, u, u_s, and u_d denote the average values over cutting periods (T_{WPM}) of the signals: i_g, v_g, i_s, v_c, v_{pv}, i_0, i_{pv}, $(v_{c_1}+v_{c_2})$, $(v_{c_1}-v_{c_2})$, μ, $(\mu_1+\mu_2)$, and $(\mu_2-\mu_1)$, respectively.

3. OBSERVER DESIGN

In this study, the Kalman observer is proposed to replace the PV sensors required to extract the voltage and current. The proposed observer allows MPP tracking the PV power without using sensors, which reduces system cost, communication burden, internal disturbances, space and complexity Das et al. (2018). Therefore, the Kalman observer adopts the following equations and variables to estimate the PV current-voltage Besancon et al. (2006) and Kissaoui et al. (2016). First, the average model (5) can be rewritten in the following compact form:

$$\dot{z} = Az + \varphi \tag{7a}$$
$$y = Pz \tag{7b}$$

with

$$A = \begin{bmatrix} 0 & 0 & 0 \\ \frac{1}{C_{pv}} & 0 & -\frac{1}{C_{pv}} \\ 0 & \frac{1}{L_0} & -\frac{r_0}{L_0} \end{bmatrix}, \varphi = \begin{bmatrix} 0 \\ 0 \\ 0.5\{u_s(w_1-1) - u_d w_2\} \end{bmatrix},$$
$$P = [0\ 0\ 1], z = [z_1\ z_2\ z_3]^T.$$

The online estimation of the PV current and voltage is performed by applying the following Kalman observer Besancon et al. (2006):

$$\dot{\hat{z}} = A\hat{z} + \varphi + D^{-1}P^T(y - P\hat{z}) \tag{8a}$$
$$\hat{y} = P\hat{z} \tag{8b}$$

with $e_0 = y - P\hat{z}$ is the observer's error. $D(0) > 0$ is any symmetric positive definite matrix; where D is definded as the solution of the following equation:

$$\dot{D} = -\rho D - A^T D - DA + P^T P, D(0) > 0 \tag{9}$$

where ρ is an arbitrary positive scalar. $\hat{z}_1$, $\hat{z}_2$, and $\hat{z}_3$ indicate the estimated values of z_1, z_2, and z_3. A, φ, and P are the same matrices given in (7).

4. CONTROLLER DESIGN

This section aims at designing a nonlinear multiloop controller to manage the energy between the PV array and the electrical grid. The control strategy is synthesized based on the ISM approach taking into account the nonlinear nature of the system. The estimated PV voltage and current are provided to the MPPT block to generate a MPP reference signal. Then, to ensure the control objectives, the ISMC is constituted based on two essential blocks, as shown in Fig. 2:

- The first block aims to ensure the MPPT reaching and the serial voltages balance.
- The second block is composed of two loops to guarantee the PFC and the regulation of DC link voltage.

4.1 PV voltage regulator design (MPPT objective)

The controller objective is to ensure the PV maximum energy. Therefore, an MPPT block is implemented to determine the MPP reference signal z_1^*, where the PV voltage z_1 should match, as closely as possible, the reference z_1^*. For this reason, an ISMC is developed. This strategy consists of the sliding surface (SS) choice and the control law design. The SMC law is generally defined as follows:

$$u_g = u_{gn} + u_{geq} \tag{10}$$

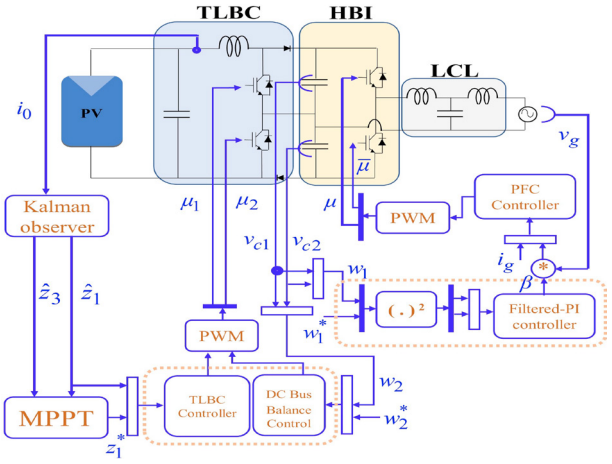

Fig. 2. Block diagram of the designed controller

where u_{geq} is the equivalent control law responsible for the sliding. u_{gn} is the switching control charged for maintaining the sliding mode along the SS.

The sliding surface: The first step in the ISMC process is the appropriate choice of the sliding function s, which is crucial to ensure the system stability. Therefore, the considered sliding variable is an integral SS that involves the tracking error, its derivative, and an integral term to avoid the time derivative of the error signal since it can increase the noise signal ratio in a practical implementation. In this sense, based on the second-order subsystem (8), the SS is presented as follows:

$$s_1 = \dot{e}_{z_1} + \lambda_1 e_{z_1} + \lambda_2 \int e_{z_1} dt \tag{11}$$

where e_{z_1} is the voltage tracking error defined as below:

$$e_{z_1} = C_{pv}(\hat{z}_1 - z_1^*) \tag{12}$$

where λ_1 and λ_2 are positive constants.

The equivalent control: Substituting (5a), (11), and (12), we obtain the first order derivative of SS :

$$\begin{aligned} \dot{s}_1 = &-\frac{1}{L_0}[\hat{z}_1 - r_0\hat{z}_2 - w_1 + 0.5(u_s w_1 - u_d w_2)] \\ &+\upsilon + e_0(m_2 - m_3) + \lambda_1(\hat{z}_3 - \hat{z}_2) \\ &-C_{pv}(m_1\dot{e}_0 + \ddot{z}_1^* + \lambda_2 e_{z_1}) - \lambda_1(m_1 e_0 + \dot{z}_1^*) \end{aligned} \tag{13}$$

where the quantities m_1, m_2 and m_3 are defined as follows:

$$m = [m_1\ m_2\ m_3] = D^{-1}P^T e_0 \tag{14}$$

As observed in equation (13), the control law u_s appears. Consequently, $u_{s_{eq}}$ can be deduced from the surface invariance $\dot{s}_1 = 0$ Otmani et al. (2017). One obtains:

$$\begin{aligned} u_{s_{eq}} = &\frac{2}{w_1}\{\lambda_2 e_{z_1} - \hat{z}_1 + r_0\hat{z}_2 + w_1 + 0.5u_d w_2 \\ &+L_0[\upsilon + e_0(m_2 - m_3) + \lambda_1(\hat{z}_3 - \hat{z}_2)]\} \\ &-\frac{2L_0C_{pv}}{w_1}\{m_1\dot{e}_0 + \ddot{z}_1^* + \lambda_1(m_1 e_0 + \dot{z}_1^*)\} \end{aligned} \tag{15}$$

The switching control: This control action has two purposes (Ensure the control law discontinuity on the SS and the control stability) El Otmani et al. (2020). To this end, the following selected Lyapunov function (LF) can be applied:

$$v_{z_1} = 0.5s_1^2 \tag{16}$$

To guarantee the control stability, it is necessary to ensure the negativity of the LF dynamics (LFD) $\dot{v}_{z_1} = s_1\dot{s}_1 < 0$, and therefore, the following expression is considered:

$$\dot{v}_{z_1} = -\alpha_1 s_1 \tanh(\frac{s_1}{\epsilon_1}) \tag{17}$$

where α_1 and ϵ_1 are positive real design parameters.

Finally, substituting (13), (15), and (17), one gets the switched control law u_{s_n}:

$$u_{s_n} = \frac{2\alpha_1 C_{pv} L_0}{w_1} \tanh(\frac{s_1}{\epsilon_1}) \tag{18}$$

4.2 DC Bus Balance Control

The balance of the voltages v_{c_1} and v_{c_2} is necessary to avoid damage to the TLBC component. Therefore, $w_2 = v_{c1} - v_{c2}$ must be null. The SS of the subsystem (6b), turns out to be:

$$s_2 = e_{w_{eq}} + \lambda_w \int e_{w_2} dt \tag{19}$$

where e_{w_2} is the tracking error defined as follows:

$$e_{w_2} = C_{eq}(w_2 - w_2^*) \tag{20}$$

where w_2^* is defined as a null reference signal, and λ_w is a positive design parameter.

Using (6b), (19) and (20), the SS dynamics turned out to be as follows:

$$\dot{s}_2 = u_d\hat{z}_2 - x_3 - C_{eq}\dot{w}_2^* + \lambda_w e_{w_2} \tag{21}$$

Then, solving (21) leads to the equivalent law :

$$u_{d_{eq}} = \frac{1}{\hat{z}_2}(x_3 + C_{eq}\dot{w}_2^* - \lambda_w e_{w_2}) \tag{22}$$

The LF and its time derivative have respectively the same form as in (16) and (17) defined follows:

$$v_{w_2} = 0.5 s_2^2 \tag{23}$$

$$\dot{v}_{w_2} = -\alpha_2 s_2 \tanh(\frac{s_2}{\epsilon_2}) \tag{24}$$

where α_2 and ϵ_2 are positive real design parameters.

Processing in the same way as the PV regulator, the switching control law is developed investigating (21), (22), and (24):

$$u_{d_n} = -\frac{\alpha_2}{\hat{z}_2} tanh(\frac{s_2}{\epsilon_2}) \tag{25}$$

4.3 Grid current regulator (PFC objective)

The DC energy is supplied to the TLBC via DC-link, which allows adjusting the HBI input to a reference higher than the grid pick voltage. As a result, a low THD current is injected into the electrical grid with a satisfactory power factor through an LCL filter. The grid current regulater is intended to provide the PFC and stabilize the subsystem (4), where the grid current must follow the reference signal x_1^*. Therefore, let us introduce the tracking error associated to the grid current as follows:

$$e_3 = L(x_1 - x_1^*) \tag{26}$$

Its second-time derivative $\ddot{e}_3$ can be expressed as follows:

$$\ddot{e}_3 = \frac{r}{L}(-rx_1 + x_2 - \bar{v}_g) + \frac{x_3 - x_1}{C} - \dot{\bar{v}}_g - L\ddot{x}_1^* \tag{27}$$

Since the relative degree of the subsystem (4) is n=3, the SS can be defined as follows:

$$s_3 = \ddot{e}_3 + \lambda_3^2 e_3 + \lambda_4 \int e_3 dt \tag{28}$$

Using (26), (27) and (28), the derivative form of SS can be expressed as follows:

$$\begin{aligned}\dot{s}_3 = &\frac{r}{L}\{2\frac{x_3 - x_1}{C} - \frac{r}{L}(x_2 - rx_1 - \bar{v}_g) - \dot{\bar{v}}_g\} \\ &+\frac{1}{LC}\{0.5(uw_1 + w_2) - 2x_2 + \bar{v}_g\} - L\dddot{x}_1^* \\ &+\lambda_4 e_3 + \lambda_3^2(x_2 - rx_1 - \bar{v}_g - L\dot{x}_1^*) - \ddot{\bar{v}}_g\end{aligned} \tag{29}$$

Solving the invariance $\dot{s}_3 = 0$, we obtain the equivalent control law:

$$\begin{aligned}u_{eq} = \frac{2LC}{w_1}\{&-2r\frac{x_3 - x_1}{LC} + \frac{r^2}{L^2}(x_2 - rx_1 - \bar{v}_g) + \ddot{\bar{v}}_g \\ &-\frac{1}{LC}(0.5w_2 - 2x_2 + \bar{v}_g - rC\dot{\bar{v}}_g) \\ &-\lambda_3^2(x_2 - rx_1 - \bar{v}_g - L\dot{x}_1^*) - \lambda_4 e_3 + L\dddot{x}_1^*\}\end{aligned} \tag{30}$$

To realize the switching control law, the following LF is considered:

$$v_3 = 0.5 s_3^2 \tag{31}$$

where α_3 and ϵ_3 are positive real design parameters.

To guarantee the LFD negativity, we must choose:

$$\dot{v}_3 = \frac{u_n}{2LC} w_1 s_3 \tag{32}$$

The switching control law is designed using (29), (30) and (32):

$$u_n = -\frac{2LC\alpha_3}{w_1} \tanh(\frac{s_3}{\epsilon_3}) \tag{33}$$

4.4 DC-Link voltage regulator

The PI linear controller is designed to generate a tuning signal β, which is intended to provide the regulation of the DC link squared voltage $y_1 = w_1^2$ to follow a desired reference y_1^*. First, the relationship between y_1 and the control signal β is defined and described in the following proposition.

Proposition: taken into consideration the system described by the average model (4-6), including the proposed observer 8, the derived control laws (15), (18), (22), (25), (30) and (33), and using the following assumptions:

- The inner loop is faster than the outer loop.
- The parasitic resistance is negligible.

The relationship between y_1 and the signal β is defined as:

$$\dot{y}_1 = \frac{4}{C_1} f_1(x) + \frac{2LC^2E}{C_1} f_2(x,t) \tag{34}$$

with

$$\begin{aligned}f_1 = &\chi_z\{L_0[\upsilon + e_0(m_2 - m_3) + \lambda_1\chi_z] + \lambda_2 e_{z1} + r_0\chi_z \\ &-L_0C_{pv}[(\dot{e}_0 + \lambda_1 e_0)m_1 + \ddot{z}_1^* - \alpha_1 \tanh\left(\frac{s_1}{\varepsilon_1}\right)] \\ &-z_1^* - \frac{e_{z1}}{C_{pv}}\},\end{aligned}$$

$$\begin{aligned}f_2 = &+\left\{C_2\dot{w}_2^* - \lambda_w e_w - \alpha_2 \tanh\left(\frac{s_2}{\varepsilon_2}\right)\right\}\frac{\chi_3}{2} - LC^2\ddot{e}_3\chi_4 \\ &\sin(\omega t)\left\{\zeta_1\frac{\chi_3}{LC^2} + 2(\zeta_1\chi_4 - \ddot{e}_3\chi_x)\right\} \\ &+2\omega\cos(\omega t)\left\{\left(\chi_4 + \frac{\chi_3}{2LC^2}\right)\chi_2 - \ddot{e}_3(\chi_1 + L\omega^2\beta)\right\} \\ &+E\omega\sin(2\omega t)\{\chi_1\chi_6 + \zeta_2 + \omega^2 L\beta(\chi_8 + \omega^2\beta L)\} \\ &+E\cos(2\omega t)\{\chi_5\chi_6 - L\beta\omega^4\chi_9 + \omega^2\zeta_3\}\end{aligned}$$

where $\chi_1 = 4r\dot{\beta} + \frac{r}{L} - 3L\ddot{\beta} - 2\left(\frac{1}{C} + \frac{r^2}{L}\right)\beta$,

$\chi_2 = 2L\dot{\beta} + r\beta + 1$, $\chi_3 = \frac{e_{w2}}{C_2} + w_2^*$, $\zeta_2 = \left(\chi_5 - \omega^2\chi_7\right)\chi_2$

$$\chi_4 = \left(\frac{r^2}{L^2} + \frac{2}{LC} - \lambda_3^2\right)\dot{e}_3 + \left(\frac{2r}{L^2C} - \lambda_4 + \lambda_3^2\frac{r}{L}\right)e_3 - 2r\frac{\ddot{e}_3}{L} - \frac{1}{2LC}\chi_3 - \alpha_3\tanh\left(\frac{s_3}{\varepsilon_3}\right)$$

$\chi_5 = \left(\frac{r^2}{L} - \frac{2}{C}\right)\dot{\beta} - \frac{1}{LC}(2r\beta + 1) + 2r\ddot{\beta} - L\dddot{\beta}$,

$\chi_6 = L\ddot{\beta} + r\dot{\beta} + \left(\frac{1}{C} - L\omega^2\right)\beta$, $\zeta_3 = \chi_6\chi_7 - L\beta\chi_5 - \chi_1\chi_2$

$\chi_7 = \left(1 - 2r\beta + 3L\dot{\beta}\right)$, $\chi_8 = 3r\dot{\beta} + \frac{r}{L} + \frac{r^2}{L}\beta - \frac{3}{C}\beta - 4L\ddot{\beta}$,

$\chi_9 = 2 - r\beta + 5L\dot{\beta}$, $\chi_x = \chi_5 + \omega^2\left(1 + 3L\dot{\beta} - 2r\beta\right)$,

$\chi_z = \hat{z}_3 - C_{pv}\dot{z}_1^* - \dot{e}_{z1} - m_1e_0$, $\zeta_1 = \chi_6 - L\omega^2\beta$.

Then, considering the fact that β and its derivatives up to order three must be available, let us present the following third-order filtered PI regulator:

$$\beta = \left(\frac{a}{a+s}\right)^3(k_{y_1}e_{y_1} + k_{y_2}e_{y_2}) \tag{35}$$

with $e_{y_1} = y - y^*$ and $e_{y_2} = \int e_{y_1}de$. where s denotes the Laplace variable and (a, k_{y_1}, k_{y_2}) are positive parameters.

5. NUMERICAL SIMULATION

This section is devoted to examining the performances and reliability of the proposed controller. The experimental setup is the controlled PV-connected grid system illustrated in Fig. 2. The simulation results of this system are investigated in Matlab/SimPowerSystems environment using the parameters listed in Tables 1 and 2. The PV module employed in the numerical simulation is of type 1Soltech 1STH-215-P. It consists of seven parallel strings and contains twelve series-connected modules per string. The MPPT block is implemented based on the INC & COND algorithm Shahid et al. (2018). The simulation tests are performed selecting the ODE1 (Euler) solver and the step time is set at $1\mu s$. The MPPT algorithm, the

Table 1. Power converters and LCL parameters

Parameters	Symbols	values
Three-level Boost	C_{pv}, L_0, r_0	1, μF, 0.45 mH, 0.01 $m\Omega$
Electrical Network	E, f	$220\sqrt{2}V$, 50 Hz
LCL-Filter	$L, C, r = r_g$	4 mH, 0.2 mF, 0.5 Ω
PWM frequency	f_{pwm}	10 Khz
DC capacitance	C_{eq}	8 mF

Table 2. Controller parametrs

Parameters	Symbols	values
Current regulator (PFC)	$\lambda_3, \alpha_3, \epsilon_3$	$1e^9, 5e^{-3}, 8e^{-3}$
Voltage regulator	$\lambda_1, \alpha_1, \epsilon_1$	$1e^{12}, 6e^{-2}, 5e^{-1}$
DC Link regulator	k_{y_1}, k_{y_2}, a	$2e^{-6}, 6e^{-5}, 1e^{-4}$
The voltage balance	α_2, ϵ_2	$6e^{-2}, 5e^{-1}$
Kalman observer parameter	ρ	$8e^3$

Kalman observer and the ISMC regulator robustness are evaluated in standard and changing climatic conditions. The performance of the resulting closed-loop control is shown in Figs. (3-6). Figs. (3-4) illustrate the simulation results in the standard conditions, while, Figs. (5-6) show the results under irradiation changes with a constant temperature maintained at 25^oC, where the solar irradiation ranges from $1000H$ to $1200H$ and decreases to $800H$ as shown in Fig. (5.a). Fig. (3.a) shows that the PV voltage reaches perfectly the MPPT and efficiently capture the maximum power corresponding to each irradiance change, as shown in Fig. (5.a). The PV current, TLBC input current, and their estimated values are illustrated in Fig. (3.b), where the PV current keeps to track the maximum value continuously even under alternating of weather conditions, as shown in Fig (5.b). Figs. (3.c) and (5.c) exhibit the DC-link voltage, which is regulated and kept constant despite the weather alternation, while the balance of v_{c_1} and v_{c_2} is ensured and their difference w_2 oscillates around a null value, demonstrating the efficiency and robustness of the ISM controller. Figs. (4.a) and (4.b) show that the current injected into the grid follows its reference and is in phase with the grid voltage. Consequently, the power factor correction in standard conditions and during irradiance changes is ensured, as shown in Figs. (6.a) and (6.b). The signal β converges after every variation to regain the supplied power rate, as illustrated in Figs. (3.d) and (4.d). Based on the FFT analysis, Fig. (4.d) shows that the grid current THD is equal to 1.43%. This value is less than 5%, which meets international standards such as IEEE1547, IEC 61727, and AS4777 Abobakr et al. (2019).

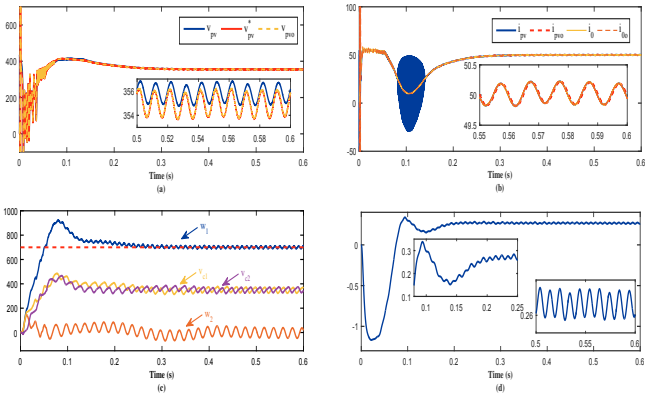

Fig. 3. (a): PV voltage, its estimated value, and the MPPT reference voltage, (b): Estimation of the PV current, (c): DC link voltage w_1 and its reference, the balance checking of v_{c1} and v_{c1}, (d): The control signal β

6. CONCLUSION

The problem of controlling a PV system connected to a single-phase grid has been addressed in this study. Accordingly, a Kalman observer was designed to estimate the PV current and voltage, and a nonlinear controller was synthesised based on the integral sliding mode approach to handle some control problems and assure a global stability of the system. The simulation results confirmed the achievement of each control objective, including ideal MPPT despite irradiation variations, power factor correction and tight regulation of the DC bus voltage.

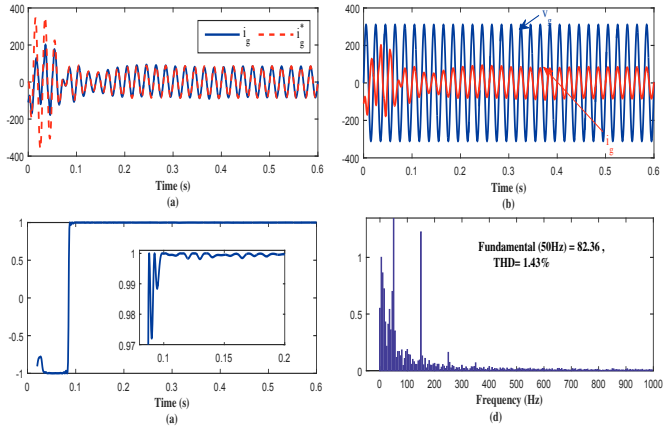

Fig. 4. (a): Grid current waveform, (b): PFC checking, (c): Power factor of the AC/DC converter, (d): Harmonic content of the grid current

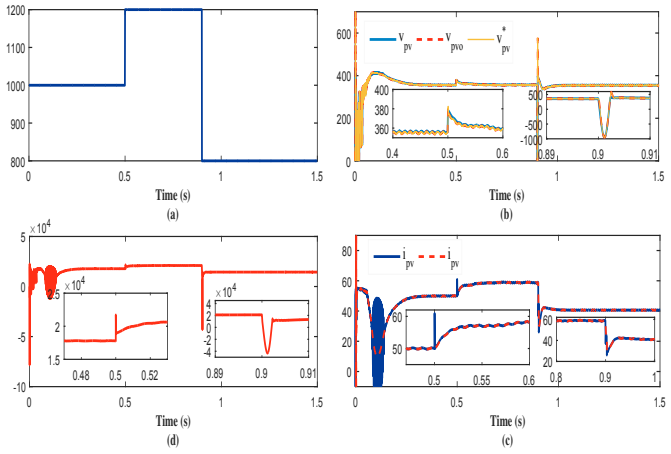

Fig. 5. (a):irradiance pattern, (b): PV voltage, its estimated value, and the MPPT reference voltage, (c): PV power, (d): Estimation of the PV current

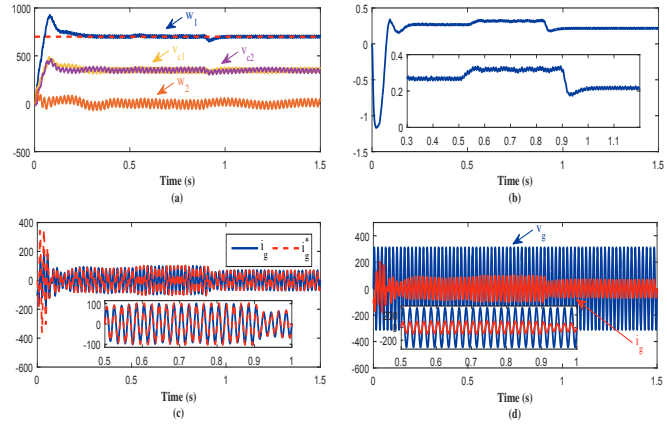

Fig. 6. (a): DC link voltage w_1 and its reference, the balance checking of v_{c1} and v_{c1}, (b): The control signal β, (c): Grid current waveform, (d): PFC checking

REFERENCES

Abobakr, H., Diab, A.A.Z., Hassan, Y.B., and AM, A. (2019). Comparison of egyptian standards for grid-connected photovoltaic power plants with iec and ieee standards: A case study in egypt. *International Journal of Advanced Science and Technology*, 28(16), 856–870.

Abouloifa, A., Aouadi, C., Lachkar, I., Boussairi, Y., Aourir, M., and Hamdoun, A. (2018). Output-feedback nonlinear adaptive control strategy of the single-phase grid-connected photovoltaic system. *Journal of Solar Energy*, 2018, 1–14.

Alik, R. and Jusoh, A. (2018). An enhanced p&o checking algorithm mppt for high tracking efficiency of partially shaded pv module. *Solar Energy*, 163, 570–580.

Aourir, M., Abouloifa, A., Lachkar, I., Aouadi, C., Giri, F., and Guerrero, J.M. (2020). Nonlinear control and stability analysis of single stage grid-connected photovoltaic systems. *International Journal of Electrical Power & Energy Systems*, 115, 105439.

Barman, S., Samanta, S., Mishra, J.P., Roy, P., and Roy, B.K. (2018). Design and implementation of an ida-pbc for a grid connected inverter used in a photovoltaic system. *IFAC-PapersOnLine*, 51(1), 680–685.

Besancon, G., de León-Morales, J., and Huerta-Guevara, O. (2006). On adaptive observers for state affine systems. *International journal of Control*, 79(06), 581–591.

Das, D., Madichetty, S., Singh, B., and Mishra, S. (2018). Luenberger observer based current estimated boost converter for pv maximum power extractiona current sensorless approach. *IEEE Journal of Photovoltaics*, 9(1), 278–286.

El Otmani, F., Abouloifa, A., Aourir, M., Lachkar, I., Assad, F., Giri, F., and Guerrero, J. (2020). Mppt based sliding mode control for fuel cell connected grid system. *IFAC-PapersOnLine*, 53(2), 13322–13327.

Kissaoui, M., Al Tahir, A., Abouloifa, A., Chaoui, F., Abouelmahjoub, Y., and Giri, F. (2016). Output-feedback nonlinear adaptive control strategy of three-phase ac/dc boost power converter for on-line ups systems. *IFAC-PapersOnLine*, 49(13), 324–329.

Otmani, F.E., Abouloifa, A., Aourir, M., Hamdoun, A., and Lachkar, I. (2017). Comparative study of two sliding surfaces to control a double boost converter. In *presented at the Proceedings of the International Conference on Industrial Engineering and Operations Management*, 1200–1201.

Shahid, H., Kamran, M., Mehmood, Z., Saleem, M.Y., Mudassar, M., and Haider, K. (2018). Implementation of the novel temperature controller and incremental conductance mppt algorithm for indoor photovoltaic system. *Solar Energy*, 163, 235–242.

Stitou, M., El Fadili, A., Chaoui, F.Z., and Giri, F. (2019). Output feedback control of sensorless photovoltaic systems, with maximum power point tracking. *Control Engineering Practice*, 84, 1–12.

Yahya, A., El Fadil, H., Oulcaid, M., Ammeh, L., Giri, F., and Guerrero, J.M. (2018). Control of grid connected photovoltaic systems with microinverters: New theoretical design and numerical evaluation. *Asian Journal of Control*, 20(2), 906–918.

Yilmaz, U., Kircay, A., and Borekci, S. (2018). Pv system fuzzy logic mppt method and pi control as a charge controller. *Renewable and Sustainable Energy Reviews*, 81, 994–1001.